Size and surface effects in the magnetic properties of maghemite and magnetite coated nanoparticles

D. Ortega, E. Vélez-Fort, D. A. García, R. García, R. Litrán, C. Barrera-Solano, M. Ramírez-del-Solar and M. Domínguez

References	**This article cites 22 articles** http://rsta.royalsocietypublishing.org/content/368/1927/4407.full.html#ref-list-1
Rapid response	**Respond to this article** http://rsta.royalsocietypublishing.org/letters/submit/roypta;368/1927/4407
Subject collections	Articles on similar topics can be found in the following collections materials science (144 articles) nanotechnology (132 articles)
Email alerting service	Receive free email alerts when new articles cite this article - sign up in the box at the top right-hand corner of the article or click **here**

To subscribe to *Phil. Trans. R. Soc. A* go to:
http://rsta.royalsocietypublishing.org/subscriptions

Size and surface effects in the magnetic properties of maghemite and magnetite coated nanoparticles

By D. Ortega[1,*], E. Vélez-Fort[2], D. A. García[2], R. García[2], R. Litrán[2], C. Barrera-Solano[2], M. Ramírez-del-Solar[2] and M. Domínguez[2]

[1]*The Davy–Faraday Research Laboratory, The Royal Institution of Great Britain, 21 Albemarle Street, London W1S 4BS, UK*
[2]*Department of Condensed Matter Physics, University of Cádiz, E11510 Puerto Real, Cádiz, Spain*

An increasing number of promising applications for future technology is arising from size constraints in nanoparticles (NPs) and from the chemical manipulation of their surfaces. In this work, we analyse the finite-size and surface effects on polyacrylic acid-coated Fe_3O_4 NPs and oleic acid-coated γ-Fe_2O_3 NPs by studying their magnetization curves at different temperatures. The measured thermal dependence of the saturation magnetization is no longer explained by the typical $T^{3/2}$ Bloch law, yielding higher values than those expected for its exponent. When incorporated in polymeric matrixes to form magnetic transparent nanocomposites, the oleic acid-coated γ-Fe_2O_3 NPs also deviate from Bloch's law, but following the opposite trend observed in free coated NPs.

Keywords: maghemite; magnetite; superparamagnetism; Bloch's law

1. Introduction

The purely structural modifications that size constraints induce in nanoparticles (NPs) and the subsequently altered atomic arrangement at their surfaces have profound consequences on their most basic physical properties. In the case of magnetic NPs, these changes have meant the departure from most of the established laws governing the magnetic phenomena observed in bulk materials for the time being. Additional chemical manipulations of NPs, such as the use of coating agents, have led to even more radical changes in the basic magnetic behaviour—turning magnetic what was not—and contributing to the enrichment of nanomagnetism by providing an increasing number of promising applications in future technology. A sizeable amount of the research done on magnetic NPs over the past decades is now starting a firm move from theoretical grounds to the real applications arena. The success in doing so is motivating the incorporation of these materials to an increasing number of fields different from those traditionally

linked to its development, such as catalysis (Yang *et al.* 2004), magneto-optical sensing (Ortega *et al.* 2006) and regenerative medicine (Solanki *et al.* 2008), to name but a few. Notwithstanding, the relentless development of improved and even more efficient materials than those currently available is further expanding the horizons of what we already knew about magnetic phenomena at the nanoscale and, moreover, where they could be applied. Even the research carried out in other areas is increasing the family of magnetic nanomaterials, a fact exemplified by some recent findings such as the onset of a ferromagnetic order in etched silicon (Grace *et al.* 2009) and hafnium dioxide (Venkatesan *et al.* 2004), two compounds where no magnetic ordering is expected to occur as a result of their electronic structure.

In addition to the obvious benefits derived from their small size, the interest in using magnetic NPs chiefly relies on their ability to be easily oriented using external magnetic fields by virtue of their *superparamagnetic* (SPM) behaviour. Well after Frenkel & Dorfman (1930) predicted the existence of *single-domain particles*, Bean & Livingston (1959) were the first in introducing the term *superparamagnetism* to designate the thermal randomization of the magnetization in fine particles—typically under 15 nm—that leads them to behave like a Langevin paramagnet (Langevin 1905) at elevated temperatures, but having a magnetic moment several orders of magnitude higher. Initially introduced by Néel (1949), the theory of superparamagnetism was subsequently developed by Brown (1963), who, instead of considering the magnetization vector pointing to a number of discrete orientations, proposed the existence of a distribution of magnetization orientations under a random field. The set of these results is known as the Néel–Brown model of the magnetic relaxation, and is widely used in studies related to the thermally activated magnetic processes both in single- and multi-particle systems. Under a practical point of view, ignoring the fluctuations associated to the magnetic moments across and at the surface of the particles, it is commonly accepted that a system of NPs is SPM when (Cullity & Graham 2009): (i) plotting the magnetization curves versus H/T (magnetic field/temperature) at different temperatures, they tend to superimpose to a single one and (ii) there is neither coercivity nor remanence, i.e. no hysteresis is observed.

Owing to their strong links with today's highest technology, the present article is focused on two similar but distinct SPM systems of iron oxide NPs with different coatings and for different applications. The first system is composed of oleic acid-coated maghemite NPs (referred as OA-γ-Fe$_2$O$_3$ NPs in the following). Apart from their uses in the form of colloids, maghemite NPs can be embedded in a range of polymeric matrixes to form transparent magnetic nanocomposites (NCs). In this article, we study their specific magnetic behaviour when incorporated in a polyester resin (OA-γ-Fe$_2$O$_3$ NC in the following). They show a high magnetic moment, but a lower optical absorption than magnetite NPs; for this reason, the main application we aim for these NPs is in magneto-optical current sensors, taking advantage of the Faraday effect that they exhibit (Ortega *et al.* 2008). The second one consists of polyacrylic acid-coated magnetite NPs (PAA-Fe$_3$O$_4$ NPs in the following), and one of its main appeals just lies in the coating agent, since PAA ensures a better dispersion in water, favouring their biocompatibility and also allowing their bioconjugation with peptides as biomarkers. In addition, the surface polarity of NPs can be easily changed to allow their transfer to non-polar solvents (Ge *et al.* 2007). Due to their high magnetic

moment and the aforementioned biocompatibility, these are excellent magnetic resonance imaging contrasts and, although in principle they had not been designed for that, magnetic hyperthermia agents as well (Kallumadil *et al.* 2009).

2. Experimental

Maghemite and magnetite SPM nanocrystals have been synthesized by two different methods based on the wet-chemical route at relatively high temperatures. In both cases, the magnetic core is formed by a chemical reaction starting from an iron precursor in the presence of a capping protective agent, to avoid excessive growing and aggregation of the clusters, using the appropriate solvents to reach the reflux temperature.

Maghemite NPs were synthesized from the thermal decomposition of iron pentacarbonyle with oleic acid as capping specie, using octyl ether as the solvent (boiling point, approx. 287°C), which allows a suitable temperature to promote the thermal decomposition of the precursor. Iron pentacabonyle was injected into a mixture of oleic acid in octyl ether, heated up to 100°C under a nitrogen flow and with vigorous stirring. The molar ratio Fe : oleic acid used in our experiment was 1 : 3. The resulting mixture was kept at the above-mentioned temperature for 1 h and then further heated up to 275°C for 90 min. After cooling to room temperature, the resulting black solution was oxidized to obtain the gamma iron oxide phase. For oxidation, trioctylamine oxide was added in a molar ratio of 3 with respect to the iron, and the mixture was heated up to 120°C in a nitrogen atmosphere for two successive heating steps. Subsequently, the temperature was increased up to 150°C for one more hour before cooling again up to room temperature. As a final step, the solution was precipitated with ethanol and dispersed again in octyl ether. The process was repeated three times to remove non-reacted species and the NPs were collected by magnetic sorting by means of an external magnetic field. Maghemite cores are surrounded by the oleic acid chains due to the coordination between carboxylate groups and iron cations on the NP surface. Oleic chains confer a hydrophobic character to the NPs, making them soluble in hydrocarbon solvents. Taking advantage of this characteristic, we have prepared transparent monolithic polyester maghemite composites appropriate for optical applications. Magnetic maghemite NPs are well dispersed in the polyester matrix; in this case, a styrene-based polymer catalysed by methyl ethyl ketone peroxide (MEKP), by *in situ* polymerization, resulting in bulk transparent polymeric composites. Three drops of MEKP were added to 1 g of polymer. The amount of NPs dissolved in the MEKP was that necessary to reach a nominal content of 1 per cent of maghemite in the polyester matrix.

Magnetite NPs were synthesized by a solution-phase hydrolysis reaction promoted by temperature. Briefly, Fe_3O_4 nanocrystals were obtained by hydrolyzing an iron precursor with an NaOH solution at a temperature above 200°C, in the presence of PAA, used as the capping agent. Specifically, a mixture of a Fe(III) precursor ($FeCl_3$) and a protective specie (PAA) was heated in dietylenglycol (DEG) up to 220°C for 30 min, in a nitrogen atmosphere while stirring. A 0.25 molar solution of NaOH in DEG, previously prepared at 120°C, was added to the reaction mixture, to promote precipitation of the hybrid iron oxide. The reaction was then refluxed for 10 min to allow the growth of magnetite

nuclei. Molar ratios of Fe : PAA and Fe : NaOH were 1 : 2 and 2 : 5, respectively. As for maghemite NPs, nanocrystal size can be tuned by modifying ratios and by increasing refluxing time. NPs were precipitated three times with ethanol, redispersed in deionized water and collected by means of an external magnetic field. Carboxylate groups in the PAA chains strongly coordinates to the iron cations on the magnetite NP surface, while uncoordinated surface carboxylate groups provides high solubility in hydrophilic solvents to the NPs, as well as a sharp capability for bioconjugation.

In both cases, magnetic nanocores surrounded by a polymeric shell have been obtained. Size distribution, as well as homogeneity and morphology of NPs have been analysed by transmission electron microscopy (TEM) using a JEOL 2010F microscope. Phase characterization has been undertaken by high-resolution transmission electron microscopy (HRTEM), complemented with inductively coupled plasma atomic emission spectroscopy (Iris Intrepid, Thermo Elemental) analysis. With regard to the processing of diffraction patterns from HRTEM images, typical tolerances of ± 0.3 nm and $\pm 3.3°$ have been employed for calculating the relationship between spacings and angles measured from the corresponding spots. Additional images have been acquired by atomic force microscopy (AFM; Veeco Multimode IIIa). Magnetic measurements have been performed in a Faraday Balance (Oxford Instruments) equipped with a liquid nitrogen cryostat. This technique belongs to the *force methods* for measuring magnetic susceptibilities and it is based on the force exerted on a suspended sample under the action of a non-uniform magnetic field. The inhomogeneity of the latter is generated by an electromagnet equipped with dedicated poles cut to a special shape known as *Faraday pole caps*, which allow a constant magnetic-field gradient region between them. The force is measured with an analytical precision balance and allows calculating the magnetization through the relationship $M = F_x[m(\mathrm{d}H/\mathrm{d}z)]$, where F_x is the force along the x direction, m the magnetic moment and $\mathrm{d}H/\mathrm{d}z$ the magnetic-field gradient between poles.

3. Results and discussion

The three sets of samples have been characterized both magnetically and morphologically. On the one hand, maghemite NPs have been characterized both as prepared and embedded in a polyester resin. On the other hand, magnetite NPs have been studied only in the 'as prepared' form. For example, figure $1a$–c shows the magnetization curves of the three samples obtained at nominal temperatures of 80 and 300 K. Obviously, the magnetization values shown in figure $1b$ are much lower than those in figure $1a$ because of the different concentration of the NPs, but, as we will show later, the fitting parameters follow the same trend. Other factors affecting the magnetic response will be discussed later.

To evaluate the SPM character of the samples and therefore to describe the field dependence of the magnetization, the experimental results at nominal temperatures between 80 and 300 K were fitted to the usual Langevin function,

$$\sigma = \sigma_s \left[\coth \frac{\mu_0 \langle \mu \rangle H}{k_B T} - \frac{k_B T}{\mu_0 \langle \mu \rangle H} \right], \tag{3.1}$$
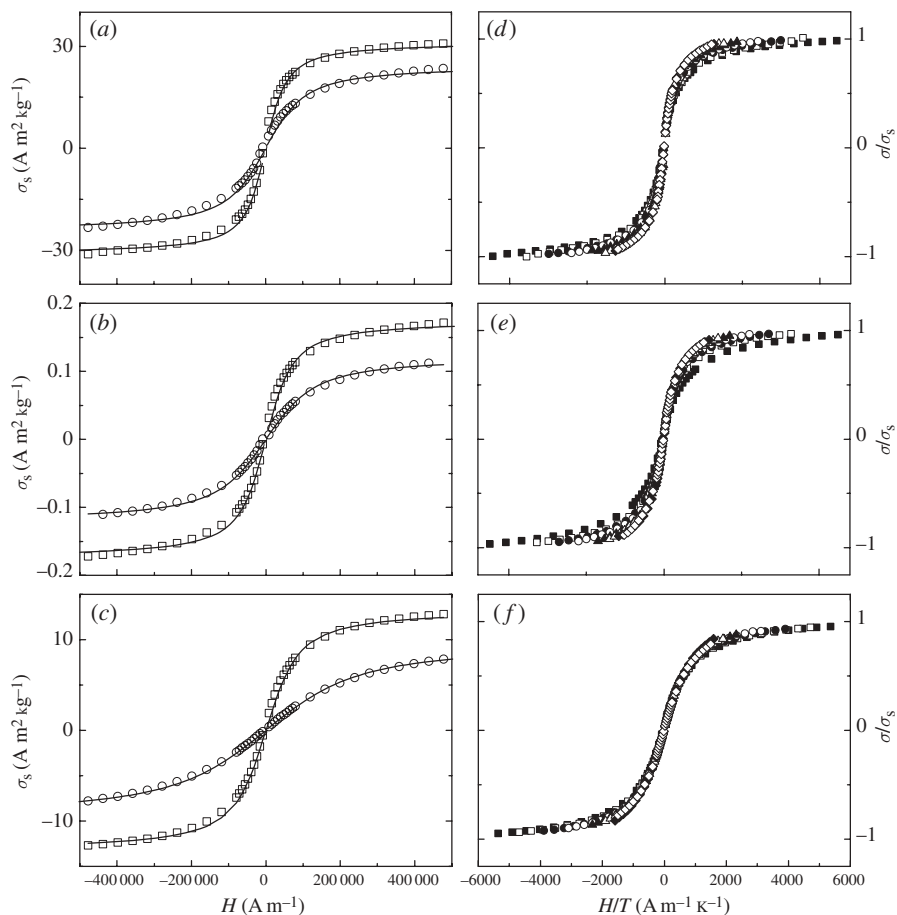
Figure 1. Magnetization curves measured at 80 and 300 K for samples: (*a*) OA-γ-Fe$_2$O$_3$ NPs, (*b*) OA-γ-Fe$_2$O$_3$ NC and (*c*) PAA-Fe$_3$O$_4$ NPs. Reduced magnetization versus H/T for samples: (*d*) OA-γ-Fe$_2$O$_3$ NPs, (*e*) OA-γ-Fe$_2$O$_3$ NC and (*f*) PAA-Fe$_3$O$_4$ NPs. (*a,b,c*) Open circle, 300 K; open square, 80 K; solid line, fit. (*d,e,f*) Filled square, 80 K; open square, 100 K; filled circle, 120 K; open circle, 150 K; filled triangle, 200 K; open triangle, 250 K; filled diamond, 300 K; open diamond, 350 K.

where σ is the specific magnetization, σ_s the specific saturation magnetization, $\langle\mu\rangle$ the NP average magnetic moment, μ_0 the magnetic permeability of vacuum and k_B the Boltzmann constant. This function basically represents the classical limit of the quantum mechanical *Brillouin function* (Cullity & Graham 2009), and its use is justified by the fact that the magnetic moments in a set of SPM NPs are larger than those of individual paramagnetic atoms, for which the Brillouin function must be employed. For each temperature between both limits and for every set of samples, the experimental data are well fitted to equation (3.1) (the correlation coefficients are all close to 0.999), which means that the NPs are essentially SPM for that temperature range. From these fits, one can obtain the saturation magnetization and the average NP diameter for each temperature. Since this diameter is deduced from the magnetization curves, we will call it the *magnetic diameter*, D_m.
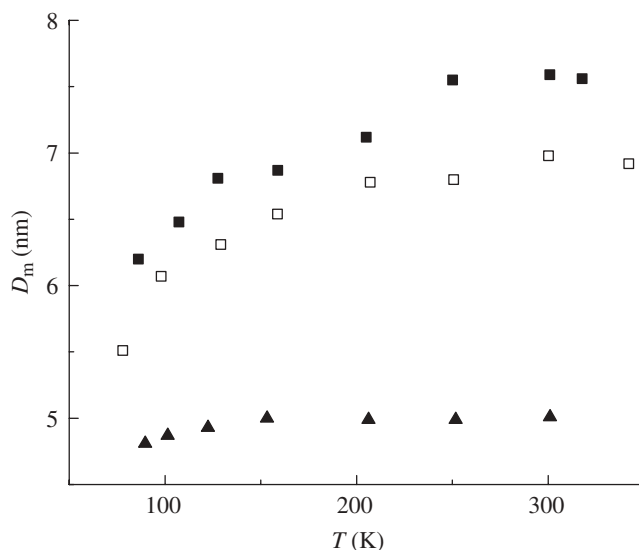
Figure 2. Magnetic diameter (D_{m}) calculated from magnetometry measurements at selected temperatures within the 80–300 K range for all studied samples. Filled square, OA-γ-Fe$_2$O$_3$ NPs; open square, OA-γ-Fe$_2$O$_3$ NC; filled triangle, PAA-Fe$_3$O$_4$ NPs.

Additionally, if the Langevin function holds as expected for SPM samples, all the measurements for a sample at the whole temperature range should collapse into a single curve. This is checked in figure 1*d–f*, where the reduced magnetization $\sigma/\sigma_{\mathrm{s}}$ is plotted versus H/T for the corresponding samples. It can be seen that this is essentially true for the magnetite sample, but not so much for the maghemite ones, especially in the lower temperature range, where the curves clearly deviate from the predicted behaviour at the region of the 'knee' of the magnetization curve. This could be interpreted as if a reduction of the size of the NPs was taking place as the temperature is reduced. Also, magnetic dipolar interactions between NPs could have a part in this departure from the H/T scaling law (Allia *et al.* 2001).

This apparent reduction in size deduced from magnetization curves becomes clearer when plotting D_{m} as a function of temperature (figure 2), where it is shown that the average size is more or less constant at the higher temperature range, but it decreases at the lower temperature range. The interpretation for this behaviour can be quite simple. Given the relatively wide size distribution of these NPs, as the temperature is decreased, those particles with a bigger size (at the right tail of the size-distribution function) may become blocked since their blocking temperature is above the temperature of this particular experiment. If they are blocked, they would not contribute to the magnetization of SPM NPs at these relatively low applied magnetic fields. The same behaviour is clearly shown in both maghemite cases (the free-NP sample and the embedded ones). In the case of magnetite samples, this effect is less visible, since it starts at a lower temperature.

The interpretation of the different behaviour shown by maghemite and magnetite samples can be followed from the size-distribution functions obtained from microscopy measurements. Figure 3*a,b* shows both TEM and HRTEM
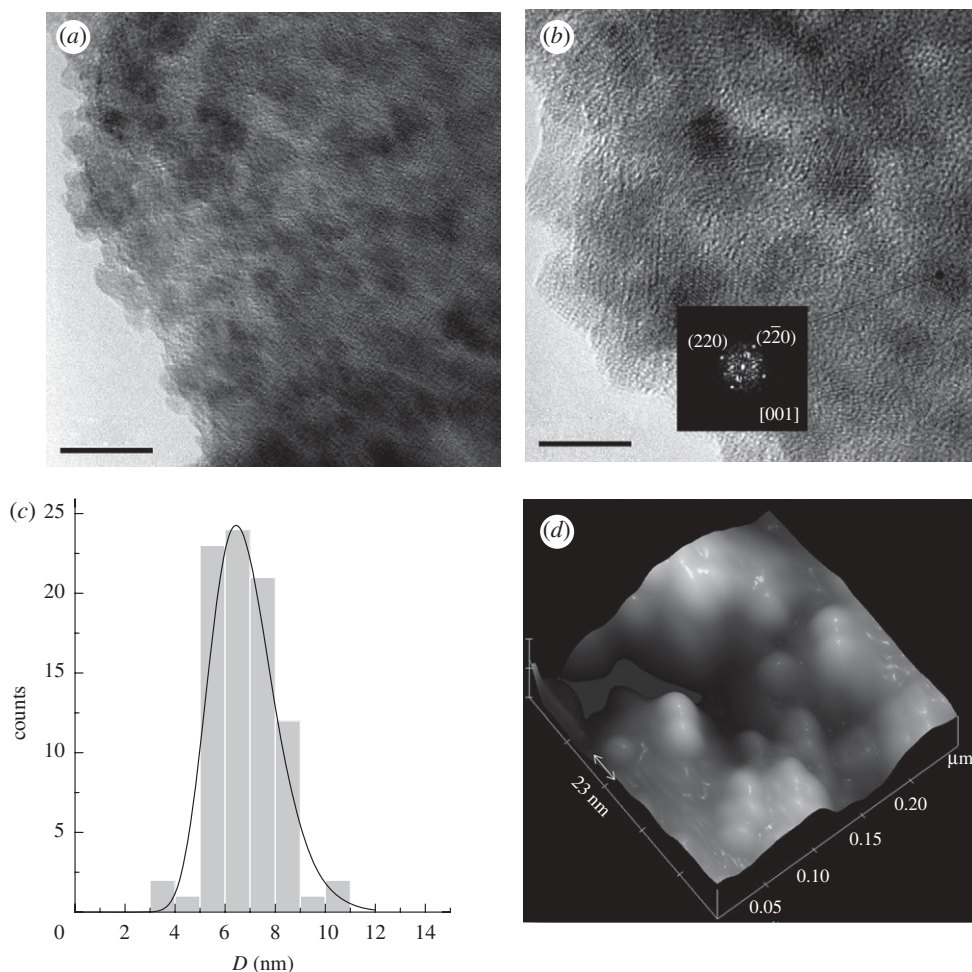
Figure 3. (a,e) TEM and (b,f) HRTEM images, (c,g) size-distribution functions and (d,h) three-dimensional AFM images of samples OA-γ-Fe$_2$O$_3$ NPs and PAA-Fe$_3$O$_4$ NPs, respectively. Zone axes are indicated between square brackets in the corresponding diffraction patterns from HRTEM images. Scale bars, (a,e) 20 nm; (b) 10 nm; (f) 5 nm.

representative images of the OA-γ-Fe$_2$O$_3$ NPs. The average core size (taken as the peak of the size-distribution function represented in figure 3c, features a value around 7 nm, although NPs with sizes ranging from 4 to 10 nm can also be observed in the TEM micrographs, i.e. there must be a considerably wide range of blocking temperatures in this case. Due to the diffuse contrast offered by the coating under the electron beam, it is difficult in this case to get the real diameter of the whole core-coating system. For comparison, an AFM image is also shown (figure 3d). Here, the diameter values (with an average around 23 nm) appear higher than those obtained through TEM, which could be connected with the fact that, in AFM measurements, the samples have been exposed to the environmental humidity; as a consequence, the surface adsorbed water makes the diameters appear bigger than expected.
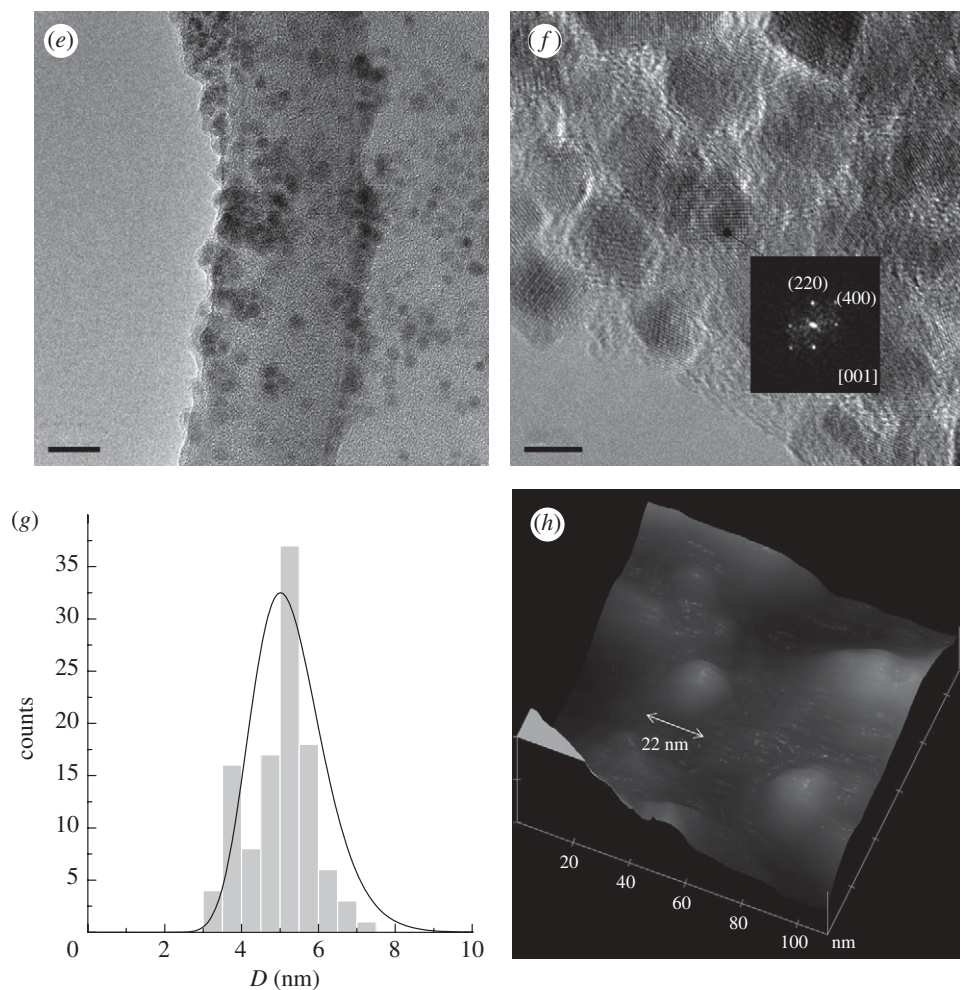
Figure 3. (*Continued.*)

One distinct feature of the PAA-Fe$_3$O$_4$ NPs, when compared with the preceding case, is that their size-distribution function is narrower than that of OA-γ-Fe$_2$O$_3$ NPs and the average size is smaller, as can be deduced from TEM and HRTEM micrographs (figure 3*e*–*g*). Figure 3*h* shows a representative AFM image of this sample revealing their spherical morphology. As occurred in the OA-γ-Fe$_2$O$_3$ NPs, the measured diameter is bigger than that obtained from TEM—now the average value is around 22 nm; furthermore, in this case, the difference between both microscopies is more pronounced, probably due to a thicker water layer over the NPs surface as a consequence of the superabsorbent character of the PAA. The different behaviour shown by the so-called magnetic diameter can then be explained by the different size distribution found for both samples. The narrower the size-distribution function, the narrower the blocking-temperatures range, which would explain why D_{m} is essentially constant until low temperatures are reached for the magnetite NPs.

Another interesting plot that may be followed from the Langevin function fits is the one for the variation of saturation magnetization with temperature. The temperature dependence of the magnetization, investigated by using a combination of different experimental methods, is an important source of information regarding the anomalies and/or singularities linked to the dimensional confinement in magnetic NPs. The deviation shown by a magnetic material if compared with its highest magnetization state is given by the spin-wave excitation. The latter is basically originated by the sinusoidal-type distribution of the spin orientation states within the material, which are forming a certain angle with respect to each other; thus, a more energetically unfavourable situation of anti-parallel coupling is avoided. Departing from the spin-wave theory, Bloch (1930) proposed an expression aiming to describe the thermal dependence of the saturation magnetization $\sigma_s(T)$ in a bulk material,

$$\sigma_s(T) = \sigma_s(0)[1 - BT^n], \tag{3.2}$$

where $\sigma_s(0)$ is the spontaneous magnetization at 0 K, n is the Bloch exponent—originally $3/2$ for bulk materials—and B is a constant that depends on the spin-wave stiffness and, thus, on the inverse of the exchange integral J. Certain deviations from the Bloch law can be observed in the case of NPs; such deviations are mainly related to the increasing of the surface to volume ratio as well as the local symmetry and exchange breaking between atoms located at the surface of these entities. This issue will be discussed later on, and its main implications compared with the outcome from our experimental measurements.

In the case of particles and clusters, some theoretical calculations have shown that the exponent n is higher than $3/2$, and may reach 2 as a consequence of the reduction in the size of the particles (Hendriksen *et al.* 1993). Going back to equation (3.2), such deviations are numerically reflected in the temperature exponent and the B constant value, which are increased with respect to the bulk values, indicating a decrease in the Curie temperature of the studied system. The main idea behind the explanation of this effect is that the lack of full coordination at the surface of the NPs may lead to larger spin deviations in this region than in the central part of the NP. The effect of the limited number of degrees of freedom at the surface leads to an energy gap in the spin-wave spectrum resulting in a flat magnetization curve at low temperatures. In other words, the magnetization decreases faster at higher temperatures in the NPs than in the bulk material, due to lacking coordination at the surface. Both Monte Carlo calculations (Merikoski *et al.* 1991) and experimental results (Senz *et al.* 2003; Caizer 2005) have repeatedly shown this behaviour.

However, there have been also reports where nanoparticulated systems show lower Bloch exponents, close to the bulk value $3/2$ (Martínez *et al.* 1998), or even lower than that (Wu *et al.* 2004).

This is the case of both free OA-γ-Fe$_2$O$_3$ and PAA-Fe$_3$O$_4$ NPs, where the best fit of the experimental results is obtained when $n = 2$ (figure 4a and b).

However, in the case of the OA-γ-Fe$_2$O$_3$ NC, the exponent from the modified Bloch law is below $3/2$, closer to 1 (table 1). For comparison, this plot is shown along with the other samples in figure 4c, and the best fit here is obtained for $n = 1.136$. These low values are justified in terms of the core-shell model for this kind of NP and the effect of the matrix where these NPs are embedded. According to this model, the magnetic NPs are composed of a single-domain core
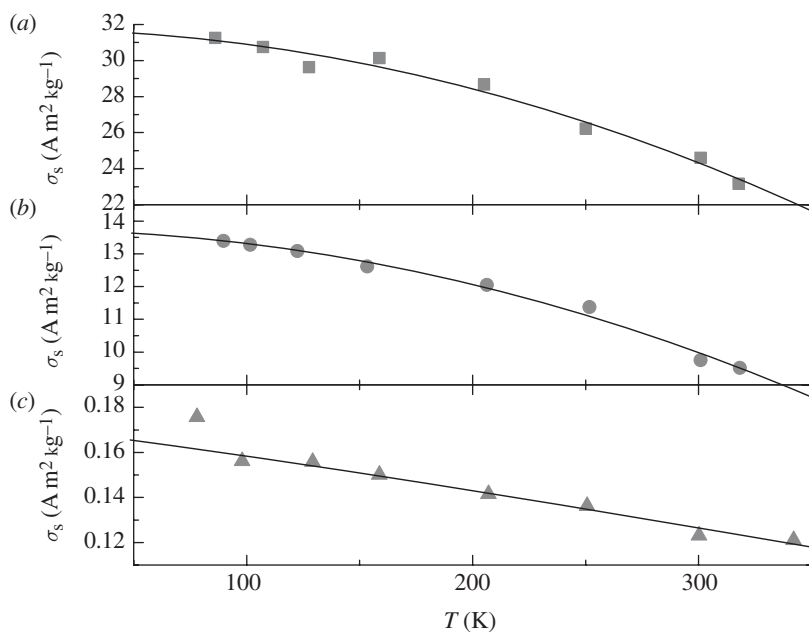
Figure 4. Comparison of the magnetization thermal dependence measured in samples: (*a*) OA-γ-Fe$_2$O$_3$ NPs, (*b*) PAA-Fe$_3$O$_4$ NPs and (*c*) OA-γ-Fe$_2$O$_3$ NC. The corresponding curve fittings to Bloch's law are represented by solid lines.

Table 1. Fitting parameters of experimental data to Bloch's law.

sample	n	$\sigma_s(0)$ (A m^2 kg^{-1})	B (K^{-n})	R
OA-γ-Fe$_2$O$_3$ NPs	2	31.72	2.59×10^{-6}	0.991
PAA-Fe$_3$O$_4$ NPs	2	13.73	3.03×10^{-6}	0.995
OA-γ-Fe$_2$O$_3$ NC	1.1	0.17	4.00×10^{-4}	0.995

that accounts for the essential magnetic behaviour of the NPs, and a shell (a more or less thick layer depending on the material and the NP size) where magnetic moments are completely disordered. A higher magnetic field is then needed to align these magnetic moments. A Bloch exponent lower than 2, according to computer simulations carried out on ferromagnetic clusters (Hendriksen *et al.* 1992), is a consequence of the fact that the shell gets thicker. When the NPs are embedded in the polyester matrix, they are subjected to high strain and it induces the growth of the magnetically disordered shell, when compared to the free NPs, at the expense of the single-domain core. Other reported examples where the Bloch exponent is 3/2 or lower for NPs include the cases where these NPs have been prepared in such a way that strains must be playing a prominent role, contributing to the overall increase in magnetic disorder; for example, NPs produced by a vaporization–condensation process (Martínez *et al.* 1998).

Another argument supporting the strain-induced core-shell magnetic structure can be followed from the inductively coupled plasma chemical analysis results. While iron oxide content in free maghemite NPs is 56.4 per cent, it is reduced to 0.87 per cent in the composite sample. If these data and the matrix diamagnetic susceptibility are used to correct the spontaneous magnetization shown in table 1, a maghemite yield of 79 per cent is inferred in the case of the free NPs, while only 30 per cent is obtained for the composite. Considering that the former NPs were used to prepare the composite, an interaction between the matrix and the NP magnetic structure must be considered in order to explain this reduction. If the disordered magnetic moments layer grows as a consequence of strains induced by the matrix, the NP saturation magnetization would be below the free NP value.

4. Conclusions

Several capped iron oxide (maghemite and magnetite) NPs have been prepared by chemical methods at high temperatures. In the case of maghemite NPs, the capping agent was oleic acid and an additional sample was prepared by encapsulating the NPs in a polyester matrix. On the other hand, the magnetite NPs were protected with a shell of hydrophilic PAA. Their magnetic properties have been studied. Magnetization curves have been fitted to the Langevin equation. A progressively better scaling in reduced magnetization (σ/σ_s) versus H/T plots (indicative of SPM behaviour) is observed from OA-γ-Fe$_2$O$_3$ NPs/NC to PAA-Fe$_3$O$_4$ NPs. The deviations from SPM behaviour can be a result from interparticle interaction, in the case of free maghemite NPs, and strains induced by the matrix, in the case of the NC.

From Langevin function plots, it is possible to deduce the NP average diameter (which we called *magnetic* diameter). These calculated magnetic diameters are not constant with temperature due to an apparent decrease that is observed at low temperatures and is more pronounced in the case of maghemite samples. Comparison of size-distribution functions deduced from TEM measurements, for both maghemite and magnetite NPs, reveals a higher mean size and wider size distribution in the first case. Therefore, the magnetic-diameter behaviour with temperature can be explained by the blocking of larger NPs as temperature decreases.

Another parameter obtained from Langevin plots is the magnetic saturation at each temperature. The results have been fitted to a Bloch-like equation. The Bloch exponents are not equal to 3/2 (the bulk value), but close to 2 for free NPs and lower than 3/2 in the case of the NC. Bloch exponents higher than 3/2 have been explained as a consequence of size reduction, but when forming NC, the exponent is close to 1 probably due to a combination of matrix-induced strains and the increase of the thickness of the disordered magnetic layer around the NPs, as shown in other nanoparticulated systems.

References

Allia, P., Coisson, M., Tiberto, P., Vinai, F., Knobel, M., Novak, M. & Nunes, W. 2001 Granular Cu–Co alloys as interacting superparamagnets. *Phys. Rev. B* **64**, 144420. (doi:10.1103/PhysRevB.64.144420)

Bean, C. P. & Livingston, J. D. 1959 Superparamagnetism. *J. Appl. Phys.* **30**, S120–S129. (doi:10.1063/1.2185850)

Bloch, F. 1930 Zur Theorie des Ferromagnetismus. *Z. Phys. A, Hadrons Nuclei* **61**, 206–219. (doi:10.1007/BF01339661)

Brown, W. F. 1963 Thermal fluctuations of a single-domain particle. *Phys. Rev.* **130**, 1677–1686. (doi:10.1103/PhysRev.130.1677)

Caizer, C. 2005 Deviations from Bloch law in the case of surfaced nanoparticles. *Appl. Phys. A* **80**, 1745–1751. (doi:10.1007/s00339-003-2471-3)

Cullity, B. D. & Graham, C. D. 2009 *Introduction to magnetic materials.* Hoboken, NJ: Wiley.

Frenkel, J. & Dorfman, J. 1930 Spontaneous and induced magnetisation in ferromagnetic bodies. *Nature* **126**, 274–275. (doi:10.1038/126274a0)

Ge, J., Hu, Y., Biasini, M., Dong, C., Guo, J., Beyermann, W. P. & Yin, Y. 2007 One-step synthesis of highly water-soluble magnetite colloidal nanocrystals. *Chem. Eur. J.* **13**, 7153–7161. (doi:10.1002/chem.200700375)

Grace, P. J., Venkatesan, M., Alaria, J., Coey, J. M. D., Kopnov, G. & Naaman, R. 2009 The origin of the magnetism of etched silicon. *Adv. Mater.* **21**, 71–74. (doi:10.1002/adma.200801098)

Hendriksen, P., Linderoth, S. & Lindgård, P. 1992 Finite-size effects in the magnetic properties of ferromagnetic clusters. *J. Magn. Magn. Mater.* **104**, 1577–1579. (doi:10.1016/0304-8853(92)91461-2)

Hendriksen, P. V., Linderoth, S. & Lindgård, P. A. 1993 Finite-size modifications of the magnetic properties of clusters. *Phys. Rev. B* **48**, 7259–7273. (doi:10.1103/PhysRevB.48.7259)

Kallumadil, M., Tada, M., Nakagawa, T., Abe, M., Southern, P. & Pankhurst, Q. A. 2009 Suitability of commercial colloids for magnetic hyperthermia. *J. Magn. Magn. Mater.* **321**, 1509–1513. (doi:10.1016/j.jmmm.2009.02.075)

Langevin, P. 1905 Magnétisme et théeorie des électrons. *Ann. Chim. Phys.* **5**, 70–127.

Martínez, B., Obradors, X., Balcells, L., Rouanet, A. & Monty, C. 1998 Low temperature surface spin-glass transition in γ-Fe$_2$O$_3$ nanoparticles. *Phys. Rev. Lett.* **80**, 181–184. (doi:10.1103/PhysRevLett.80.181)

Merikoski, J., Timonen, J., Manninen, M. & Jena, P. 1991 Ferromagnetism in small clusters. *Phys. Rev. Lett.* **66**, 938–941. (doi:10.1103/PhysRevLett.66.938)

Néel, L. 1949 Théorie du traînage magnétique des ferromagnétiques en grains fins avec applications aux terres cuites. *Ann. Geophys.* **5**, 99–136.

Ortega, D., Garitaonandia, J. S., Barrera-Solano, C., Ramírez-del-Solar, M., Blanco, E. & Domínguez, M. 2006 γ-Fe$_2$O$_3$/SiO$_2$ nanocomposites for magneto-optical applications: nanostructural and magnetic properties. *J. Non-Cryst. Solids* **352**, 2801–2810. (doi:10.1016/j.jnoncrysol.2006.03.056)

Ortega, D., García, R., Marín, R., Barrera-Solano, C., Blanco, E., Domínguez, M. & Ramírez-del-Solar, M. 2008 Maghemite–silica nanocomposites: sol–gel processing enhancement of the magneto-optical response. *Nanotechnology* **19**, 475706. (doi:10.1088/0957-4484/19/47/475706)

Senz, V., Röhlsberger, R., Bansmann, J., Leupold, O. & Meiwes-Broer, K. H. 2003 Temperature dependence of the magnetization in Fe islands on W(110): evidence for spin-wave quantization. *New J. Phys.* **5**, 47. (doi:10.1088/1367-2630/5/1/347)

Solanki, A., Kim, J. D. & Lee, K. B. 2008 Nanotechnology for regenerative medicine: nanomaterials for stem cell imaging. *Nanomedicine* **3**, 567–578. (doi:10.2217/17435889.3.4.567)

Venkatesan, M., Fitzgerald, C. B. & Coey, J. M. D. 2004 Unexpected magnetism in a dielectric oxide. *Nature* **430**, 630. (doi:10.1038/430630a)

Wu, M., Zhang, Y., Hui, S., Xiao, T., Ge, S., Hines, W. & Budnick, J. 2004 Temperature dependence of magnetic properties of SiO$_2$-coated Co nanoparticles. *J. Magn. Magn. Mater.* **268**, 20–23. (doi:10.1016/S0304-8853(03)00412-8)

Yang, H. H., Zhang, S. Q., Chen, X. L., Zhuang, Z. X., Xu, J. G. & Wang, X. R. 2004 Magnetite-containing spherical silica nanoparticles for biocatalysis and bioseparations. *Anal. Chem.* **76**, 1316–1321. (doi:10.1021/ac034920m)